Anal. Chem. **2002,** *74,* 3991−4001

Cell Docking and On-Chip Monitoring of Cellular Reactions with a Controlled Concentration Gradient on a Microfluidic Device

Mengsu Yang,* Cheuk-Wing Li, and Jun Yang

Applied Research Centre for Genomic Technology and Department of Biology and Chemistry, City University of Hong Kong, 83 Tat Chee Avenue, Kowloon, Hong Kong SAR, China

We have developed a microfluidic device for on-chip monitoring of cellular reactions. The device consists of two primary analytical functions: control of cell transport and immobilization, and dilution of an analyte solution to generate a concentration gradient. In this device, a dam structure in parallel to the fluid flow was constructed for docking and alignment of biological cells, which allows the fragile cells to move in the microfluidic channels and to be immobilized with controllable numbers in desired locations. The cells docked on the parallel dam structure are exposed to minimal stress caused by fluidic pressure. Additionally, a network of microfluidic channels was designed to generate a concentration gradient by controlled fluid distribution and diffusive mixing. An analyte solution could be diluted to different gradients as a function of distance along the dam. We used the ATP-dependent calcium uptake reaction of HL-60 cells as a model for on-chip measurement of the threshold ATP concentration that induces significant intracellular calcium signal. The results have demonstrated the feasibility of using the microchip for real-time monitoring of cellular processes upon treatment of a concentration gradient of a test solution. The integration of cell manipulation and solution manipulation on a microchip allows the measurement of concentration-dependent biological responses within a confined microscale feature.

The ability to fabricate microscale analytical structures on planar substrates with high performance and the similar dimensions between the structural components of microfluidic devices and biological cells have attracted significant attention in the development of microchips for analysis of biophysical and biochemical functions of cells.[1−11] Controlled transport, immobilization, and manipulation of biological molecules and cells, as well as controlled manipulation of reagents such as separation, mixing, and dilution, are important functions to be incorporated into a microfluidic device in order to carry out on-chip biochemical and cell biological experiments.

Previous studies have demonstrated the feasibility of handling biological cells on microfluidic devices by using various physical forces.[1−4] For example, Li and Harrison used electroosmotic and electrophoretic pumping to select and transport cells within a network of capillary channels, where various on-chip manipulations such as plug formation in double-T intersections, flow switching between branches in a Y-shaped channel, and cell lysing experiments by SDS were demonstrated.[1] The self-adhering property of white blood cells has been utilized to trap and fractionate granulocyte and lymphocyte subtypes within a variable-length channel array with channel diameter slightly smaller than target cells.[2] Other customized channel architectures have been developed for the purpose of cell immobilization, such as the constriction structures for single embryonic cell entrapment[5] and the weir structure for retaining solid beads.[6] In general, the trapping mechanism of these architectures is by narrowing down the fluidic pathway at a particular region of a microfluidic device to a size smaller that the dimension of the particles in order to retain the interested particles while allowing the fluid to flow through. An alternative to trapping cells by modified channel architectures is to control particle manipulation by negative dielectrophoresis (nDEP).[7] It has been shown that, depending on the electrode array structure, analytical functions of funnel, aligner, cage, and switch modules could be performed and controlled by ac currents. This technique allows gentle fluid manipulation that is critical to avoid mammalian cell distortion while cells are levitated and contact-free in solution. However, efficient particle trapping by nDEP requires very low flow rate (in the μL/h range).[7] Fabrication and

* Corresponding author: (e-mail) bhmyang@cityu.edu.hk; (fax) 852-2788-7406.

(1) Li, P. C. H.; Harrison, D. J. *Anal. Chem*. **1997**, *69*, 1564−1568.
(2) Carlson, R. H.; Brody, J. P.; Chan, S.; Gabel, C.; Winkleman, J.; Austin, R. H. *Phys. Rev. Lett*. **1997**, *79*, 2149−2152.
(3) Waters, L. C.; Jacobson, S. C.; Kroutchinina, N.; Khandurina, J.; Foote, R. S.; Ramsey, J. M. *Anal. Chem*. **1998**, *70*, 158−162.
(4) Blankenstein, G.; Larsen, U. D. *Biosens. Bioelectron*. **1998**, *13*, 427−438.
(5) (a) Glasgow, I. K.; Zeringue, H. H.; Beebe, D. J.; Choi, S. J.; Lyman, J. T.; Wheeler, M. B. *Micro-Total Analysis Systems' 98* **1998**, 199−202. (b) Beebe, D. J.; Glasgow, I. K.; Wheeler, M. B. Microfluidic embryo and/or oocyte handling device and method. U.S. Patent 6,193,647, 1999.
(6) Oleschuk, R. D.; Shultz-Lockyear, L. L.; Ning. Y.; Harrison, D. J. *Anal. Chem*. **2000**, *72*, 585−590.
(7) Muller, T.; Gradl, G.; Howitz, S.; Shirley, S.; Schnelle, T.; Fuhr, G. *Biosens. Bioelectron*. **1999**, *14*, 247−256.
(8) (a) Vo-Dinh, T.; Alarie, J. P.; Isola, N.; Landis, D.; Wintenberg, A. L.; Ericson, M. N. *Anal. Chem*. **1999**, *71*, 358−363. (b) Falsey, J. R.; Renil, M.; Park, S.; Li, S.; Lam, K. S. *Bioconjugate Chem*. **2001**, *12*, 346−353.
(9) Kwok, Y. C.; Jeffery, N. T.; Manz, A. *Anal. Chem*. **2001**, *73*, 1748−1753.
(10) McClain, M. A.; Culbertson, C. T.; Jacobson, S. C.; Ramsey, J. M. *Anal. Chem*. **2001**, *73*, 5334−5338.
(11) Tamaki, E.; Sato, K.; Tokeshi, M.; Sato, K.; Aihara, M.; Kitamori, T. *Anal. Chem*. **2002**, *74*, 1560−1564.

10.1021/ac025536c CCC: $22.00
Published on Web 07/23/2002

alignment of three-dimensional microelectrode systems are also complicated.

Another area of particular interest is the on-chip mixing and generation of a concentration gradient of analyte solutions.[12−20] Analyte concentration is an important parameter in every chemical or biochemical reaction. Usually, serial dilution experiments with ascending/descending concentrations are carried out to evaluate the optimal concentration (range) for a particular chemical to most effectively function on a biological system. Attempts have been made to generate discrete concentrations on microfluidic devices, usually by joining analyte and buffer streams followed by parallel or serial diffusive mixing.[12−14] It has been shown that a concentration gradient in parallel to fluidic flow in a short straight channel could be generated by diffusion before the analyte and the buffer were equilibrated within the microchannel.[16] Recently, Whitesides et al. described the generation of concentration gradients having complex shapes in solution using microfluidic networks.[17,18] In the tree-like microfluidic network, analyte is equilibrated in the mixed stream prior to subsequent splitting and mixing, where the length of the mixing channel should provide sufficient time for diffusion. Gradients perpendicular to flow could be achieved by repeatedly splitting, mixing, and recombining streams of analyte and buffer solutions.[18] However, most of microfluidic designs aimed at reducing the effect of diffusion[20] rather than utilizing the diffusive mixing as a means to generate concentration gradients.

In this paper, we described the development of a microfluidic device for on-chip monitoring of cellular reactions. The device consists of two primary analytical functions: control of cell transport and immobilization, and dilution of an analyte solution to generate a concentration gradient. In this device, a dam structure in parallel to the fluid flow was constructed for docking and alignment of biological cells. The structure allows the cells to move in the microfluidic channels and dock in desired locations with controllable number. The cells docked on the parallel dam structure are exposed to minimal stress caused by fluidic pressure. In addition, the network of microfluidic channels was designed to generate a concentration gradient by controlled fluid distribution and diffusive mixing. An analyte solution could be diluted to different gradients as a function of distance along the dam. We have used the ATP-dependent calcium uptake reaction of HL-60 cells as a model for on-chip measurement of the threshold ATP concentration that induces significant intracellular calcium signal. The results have demonstrated the feasibility of using the microchip for real-time monitoring of cellular processes upon treatment of a concentration gradient of a test solution. The integration of cell manipulation and solution manipulation on a microchip allows the measurement of concentration-dependent biological responses within a confined microscale feature.

EXPERIMENTAL SECTION

Cells and Reagents. Suspension HL-60 cells (human promyelocytic leukemia) were cultured in a sterile flask. Culture medium was prepared by RPMI 1640 with L-glutamine (Gibco-BRL), 10% (v/v) fetal bovine serum (Gibco-BRL), and 1% (v/v) penicillin−streptomycin (Gibco-BRL) with pH adjusted to 7.4. Standard Hank's balanced salt solution (HBSS, Gibco-BRL) containing calcium was used for cell loading and on-chip experiments. Fluo3-AM (Calbiochem) stock solution (1 mM) was prepared in dry dimethyl sulfoxide (Calbiochem). A 20% (w/v) Pluronic F-127 (Molecular Probes) stock solution was prepared in dry dimethyl sulfoxide (DMSO). Adenosine 5′ triphosphate (ATP) stock solution (20 mM) from equine muscle (crystalline disodium salt, Sigma) was freshly prepared in HBSS before the experiments. For acridine orange (AO, Sigma) and ethidium bromide (EB, Molecular Probes) related studies, PBS buffer was used as the solvent and its pH was adjusted to 7.4. AO/EB (50 μg/mL AO, 50 μg/mL EB) stock solution was prepared for cell staining (with 200 ng/mL working concentration for both dyes), and 33 μM AO was used in the dye flow study. All solutions except the culture medium were filtered by disposable syringe filters (MFS 25, Advantec MFS, Inc) with a pore size of 0.25 μm before use.

Microchip Fabrication and Operation. The microfluidic device was constructed from a quartz etched plate sealed with poly(dimethylsiloxane) (PDMS) by conformal contact.[21] The quartz plate was fabricated by Shanghai Institute of Metallurgy, Chinese Academy of Sciences using a traditional photolithography method followed by HF wet etching.[22] Two photomasks were used to create the microfluidic device: the first was used to etch the tops of the dam structure to a depth of 5 μm followed by a second etching procedure to etch the channels to 19.3 μm in depth. PDMS was prepared in 10:1 silicone elastomer with curing agent (Sylgard 184, Dow Corning, Midland, MI) according to a published protocol.[21] All experiments were performed on a single microfluidic device as illustrated in Figure 1. Before experiments, the etched quartz plate and a PDMS cover were touch-bonded and irradiated with UV light for 10 min in a biosafety cabinet. After filling the microchannels with buffer by capillary action, the device was securely mounted on the stage of a confocal microscope. Introduction of various fluids was implemented by using 2−20 μL pipets.

Liquid Level Program (LLP). The liquid level program is a specific combination of liquid levels at the six inlet/outlet vials of the microchip (Figure 1a). Different volumes of reagent were loaded into the vials to create liquid level differences that determined the net fluidic flow direction and fluidic pressure within the microchannels. The liquid level difference was varied for different experiments (Table 1).

(12) Harrison, D. J.; Fluri, K.; Seiler, K.; Fan, Z.; Effenhauser, C. S.; Manz, A. *Science* **1993**, *261*, 895, 897.

(13) (a) Kutter, J. P.; Jacobson, S. C.; Ramsey, J. M. *Anal. Chem.* **1997**, *69*, 5165−5171. (b) Kutter, J. P.; Jacobson, S. C.; Matsubara, N.; Ramsey, J. M. *Anal. Chem.* **1998**, *70*, 3291−3297.

(14) Jacobson, S. C.; McKnight, T. E.; Ramsey, J. M. *Anal. Chem.* **1999**, *71*, 4455−4459.

(15) (a) Kenis, P. J.; Ismagilov, R. F.; Whitesides, G. M. *Science* **1999**, *285*, 83−85. (b) Takayama, S.; McDonald, J. C.; Ostumi, E.; Liang, M. N.; Kenis, P. J.; Ismaglov, R. F.; Whitesides, G. M. *Proc. Natl. Acad. Sci. U.S.A.* **1999**, *96*, 5545−5548.

(16) (a) Darling, R. B.; Yager, P.; Weigl, B.; Kriebel, J.; Mayes, K. *Micro-Total Analysis Systems' 98*, **1998**, 105−108. (b) Kamholz, A. E.; Weigl, B. H.; Finlayson, B. A.; Yager, P. *Anal. Chem.* **1999**, *71*, 5340−5347.

(17) Jeon, N. L.; Dertinger, S. K. W.; Chiu, D. T.; Choi, I. S.; Stroock, A. D.; Whitesides, G. M. *Langmuir* **2000**, *16*, 8311−8316.

(18) Dertinger, S. K. W.; Chiu, D. T.; Jeon, N. L.; Whitesides, G. M. *Anal. Chem.* **2001**, *73*, 1240−1246.

(19) Mitchell, M. C.; Spilmans, V.; Bessoth, F.; Manz, A.; Mello A. de. *Micro-Total Analysis Systems' 2000* **2000**, 463−465.

(20) Dutta, D.; Leighton, D. T. *Anal. Chem.* **2002**, *74*, 1007−1016.

(21) Delamarche, E.; Bernard, A.; Schmid, H.; Bietsch, A.; Michel, B.; Biebuyck, H. *J. Am. Chem. Soc.* **1998**, *120*, 500−508.

(22) Fan, Z. H.; Harrison, D. J. *Anal. Chem.* **1994**, *66*, 177−184.

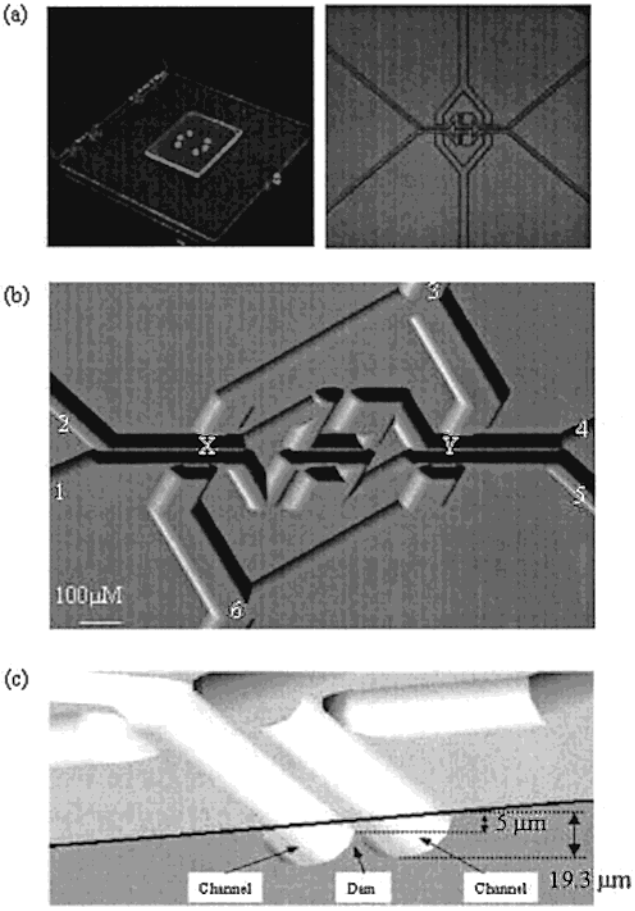

Figure 1. Microchip design for on-chip monitoring of cellular reactions. (a) Left: Photograph of the microfluidic device used in this study. There are six holes (reservoirs) as inlets/outlets for loading solution and collecting waste. Right: Top-down 2D view (CAD image) of the microfluidic design in this microdevice. (b) 3D view (CAD image) of the main features (channels, dams and intersections) in this microdevice. Channels numbered with 1−6 are extended to their corresponding reservoirs. Points X and Y are intersections where analyte and buffer solutions converge. The channel sections before X, between X and Y, and after Y are labeled as A−B, C−D, and E−F, respectively. The line feature between channels 1−5 and channels 2−4 is a dam structure for cell docking. (c) Cross section of the microchip showing the dimensions of the channels and the dam structure.

Fluorescence Image Acquisition. A confocal laser-scanning microscope (Axiovert 100M, Carl Zeiss) was used for data acquisition. The profiling data analysis mode was employed to present the PMT response along a specific line in a particular microchannel. All fluorophores (AO, EB, Fluo3) were excited by an argon laser (488 nm). The emission filter of 505−530 nm was used for Fluo3 and AO, and the long-pass (560 nm) filter was used for EB. Scanning parameters were kept constant throughout all experiments for a particular fluorophore.

Procedures. Three sets of experiments were performed on the microfluidic device. The first set of experiments involved the transport and immobilization of cells, with a standard AO/EB staining assay to examine the viability of the docked cells. The second set of experiments involved the generation of concentration gradients using a fluorescence dye (AO) and different liquid level programs. Once both cell docking and dilution functions were demonstrated feasible, the third set of experiments was carried out by combining the cell docking and gradient generation to determine the threshold ATP concentration for inducing a calcium signaling reaction. A serial dilution experiment was also conducted to obtain the threshold ATP concentration by conventional cell-based assay.

Cell Docking and Viability Test. HL-60 cells were resuspended in 0.5 mL of fresh RPMI 1640 medium with Pluronic F-127 (1% w/v final)[23] and Fluo3-AM (2 μM final concentration).[24] After 30 min of incubation at room temperature, cells were resuspended in HBSS medium before loading into the microfluidic device. Cells were loaded according to the LLP-A (Table 1) with PBS buffer as the mobile phase. After cells were fully docked, the LLP was changed to B (Table 1), where reservoir 1 was loaded with 10 μL of PBS. AO/EB staining was performed 20 min after cell docking by using LLP-B.

Generation of Concentration Gradients. A 33 μM AO dye solution in PBS buffer was prepared to generate concentration gradients. Two gradients were generated with different liquid levels in various inlets using the LLP C1 (termed simple dilution mode) and LLP C2 (termed complex dilution mode) according to Table 1, respectively. Confocal fluorescence images were acquired 2 min after the dye solution was loaded in vial 1. The profile data analysis mode was utilized to retrieve fluorescence intensity responses along specific lines in the microchannels. For the purpose of cell intensity measurement, the lines were usually taken at a distance of 10 μm from the dam structure on which cells were to be docked.

Threshold Concentration of ATP-Dependent Calcium Uptake. First, cells previously incubated with Fluo3-AM were docked on the channel as mentioned above. Once the docking process was completed, LLP was switched to D (Table 1) where HBSS solution was used as the buffer. Various concentrations (2, 5, and 10 μM) of ATP solution was injected into vial 1 sequentially with 2-min HBSS washing at intervals. Confocal fluorescence images were taken 2 min after the introduction of ATP. Profile data analysis mode was used to acquire fluorescence intensity of the line at 10-μm distance from the dam structure where cells (~15 μm in diameter) were docked on it. The fluorescence intensity of individual cells docked along the dam was obtained as plotted as a function of distance. A solution-based fluorescence assay was used to estimate the threshold ATP concentration independently. Individual experiments were performed after Fluo3-AM-treated HL-60 cells were exposed to various ATP concentrations (μM): 0.001, 0.01, 0.04, 0.05, 0.1, 0.15, 0.2, 0.25, 0.3, 0.35, 0.4, 0.45, 0.5, 1, 10, 100, and 1000. The fluorescence intensity of cells on thoroughly washed glass slides treated with different ATP concentration was measured by the confocal fluorescence microscope.

RESULTS AND DISCUSSION

Design Principle of the Parallel Dam Structure. Several channel architectures were previously developed for the purpose of cell immobilization, such as the constriction structures[5] and the weir structures[6] for cell entrapment. The trapping "dam" structure is usually constructed perpendicular to the liquid flow route and is referred to as a "perpendicular dam". The dam

(23) Lin, K.; Sadee, W.; Quillan, J. M. *BioTechniques* **1999**, *26*, 318−326.
(24) Thomas, D.; Tovey, S. C.; Collins, J.; Bootman, M. D.; Berridge, M. J.; Lipp, P. *Cell Calcium* **2000**, *28*, 213−223.

Table 1. Liquid Level Program (LLP) Used in Fluid Manipulations[a]

LLP	operation mode	liquid volume (solution or buffer) in individual reservoir (μL)					
		1	2	3	4	5	6
A	cell loading and docking	0	0	0	4 (PBS)	5 (cells)	20 (PBS)
B	AO/EB staining	10 (AO/EB)	10 (PBS)	10 (PBS)	0	0	10 (PBS)
C1	simple dilution	5 (AO)	5 (PBS)	15 (PBS)	0	0	15 (PBS)
C2	complex dilution	5 (AO)	0	20 (PBS)	0	0	20 (PBS)
D	ATP-dependent calcium uptake	5 (ATP)	0	20 (HBSS)	0	0	20 (HBSS)

[a] Abbreviations: AO, acridine orange; EB, ethidium bromide; ATP, adenosine triphosphates; PBS, phosphate-buffered saline solution; cells, HL-60 cells; HBSS, Hank's balanced salt solution.

structure for cell immobilization described in this paper is constructed in parallel to the liquid flow route and is referred to as a "parallel dam".

We have attempted to immobilize cells on a perpendicular dam structure using hydrodynamic force for transporting cells. While it was possible to trap cells with the perpendicular dam, several disadvantages were noted during the immobilization and to carry out subsequent on-chip bioassays after the immobilization, particularly for mammalian cells. First, fragile mammalian cells were subjected to distortion when stopped at a perpendicular dam due to liquid pressure. The increase in the number of immobilized cells at the dam resulted in a narrower passage for the liquid flow, causing the shear flow rate near the cells to increase. Consequently, the hydrodynamic pressure on the immobilized cells was also increased. Cells would even squeeze through the dam structure when the pressure was further increased, making cell conditions unstable for biological assays.[25] A reduction in the main flow rate would lead to significant increase in the time required to transport cells from the inlet to the dam, making rapid measurement impossible. (A video clip is not available.) Second, it is difficult to control the hydrodynamic pressure applied on the cells on the perpendicular dams. Rapid cell transportation requires increasing liquid pressure; however, unlike rigid glass beads, severe damage to fragile mammalian cells would occur when cells crash onto the perpendicular dam under high flow rate and high static pressure. On the other hand, if liquid pressure is decreased in order to reduce cell damage and clogging at perpendicular dams, the flow rate becomes very slow for cell transportation from the injection vial to the dam. In addition, low liquid pressure is also attributed to causing serious cell adhesion on the microchannels.[1] Finally, cells trapped by the perpendicular dam tended to aggregate and form multiple layers, making it difficult to control the number of cells immobilized in each run. The fluidic flow varies with the amount of particles immobilized, and the resistance changes drastically after the dam is completely clogged. As a result, it is difficult to carry out accurate and reproducible cell-based measurements. Because of the difficulties in creating efficient cell transportation with gentle cell immobilization, successful handling of mammalian cells with perpendicular dam structures is rarely reported.

To address some of the problems of the perpendicular dam during mammalian cell immobilization and measurement, we have constructed a microfluidic device consisting of a parallel dam structure. Figure 1 shows the overall design and the dimensions of the channels and dam structure of the microchip. The overall size of the microchip is 5 cm (length) $\times$ 4 cm (width) $\times$ 0.5 cm (height). There are six holes (reservoirs or vials) serving as inlets/outlets for six microchannels, respectively, for sample injection and waste collection. The main features of the design include a parallel dam structure (Figure 1c) for cell immobilization and a network of microfluidic channels and intersections for generation of concentration gradients (Figure 1b).

The parallel dam structure is composed of two parallel channels separated by a dam, where the height of the dam is smaller than the vertical height of the channels (Figure 1c). The gap between the two channels is $\sim$5 μm, smaller than the diameters of most mammalian cells. The design principle behind the parallel dam structure for cell docking, alignment, and immobilization is illustrated in Figure 2. The parallel dam allows liquid to flow over from one channel to the other but prevents cells from passing through. When liquid pressure in one channel (channel 5 in Figure 2) is higher than the other channel (channel 4 in Figure 2), a fraction of the fluid flows over the dam structure. The hydrodynamic pressure difference will bring the cells in channel 5 to dock along the dam (thus termed "cell docking"). When cells are docked along the dam to block a certain position of the gap, the flow will be attenuated at the position and other cells will only dock at other available positions along the dam. Only cells running closer to the channel wall (laminas of slower velocities) near the dam will be driven by the small pressure difference to dock gently against the dam. (A video clip showing the docking of HL-60 cells at a parallel dam structure is given as Supporting Information.) Liquid pressure will not increase significantly on cells, as the main flow route is not blocked at all. When the dam is fully docked, the immobilized cells occupy the region close to the channel wall so that it becomes more difficult for excessive cells to approach the laminas of slower velocities near the dam and they are driven away along the main flow route. As a result, a single line of cells will be docked along the dam without multilayer formation. Therefore, it is possible to control the number of cells immobilized on the microchannel.

Cell Docking at a Parallel Dam. Figure 3 shows the photographic and fluorescence images of HL-60 cells after complete docking to form a line of immobilized cells at a parallel dam of the microfluidic device. It can been seen that HL-60 cells

(25) Yang, M.; Li, C. W., unpublished results.

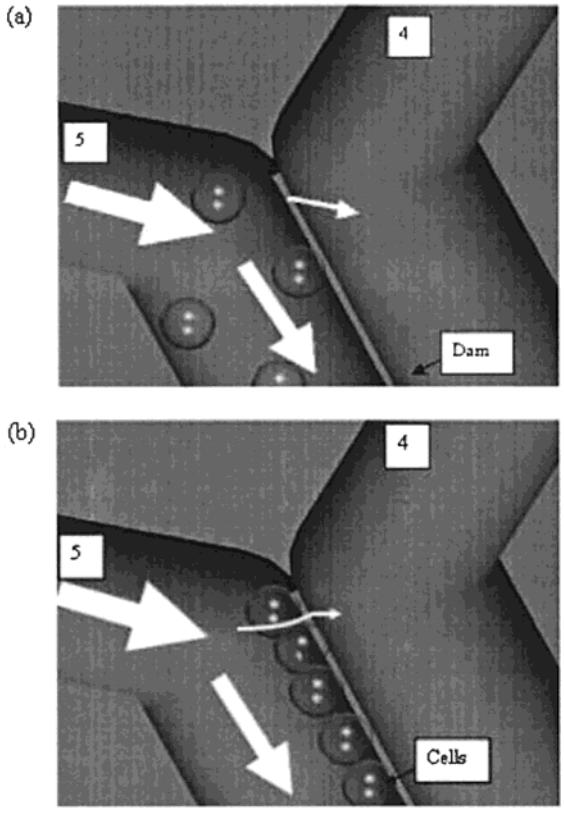

Figure 2. Schematic diagrams of the fluid flow during cell docking. (a) When liquid pressure in channel 5 is higher than in channel 4, a fraction of the fluid flows over the dam structure to channel 4. The hydrodynamic pressure difference will bring the cells in channel 5 to dock along the dam. (b) After complete cell docking, the fraction of flow across the dam is reduced so that excessive cells become more difficult to approach the laminas of slower velocities near the dam and are driven away along the main flow route. A single line of cells will be docked along the dam without multilayer formation.

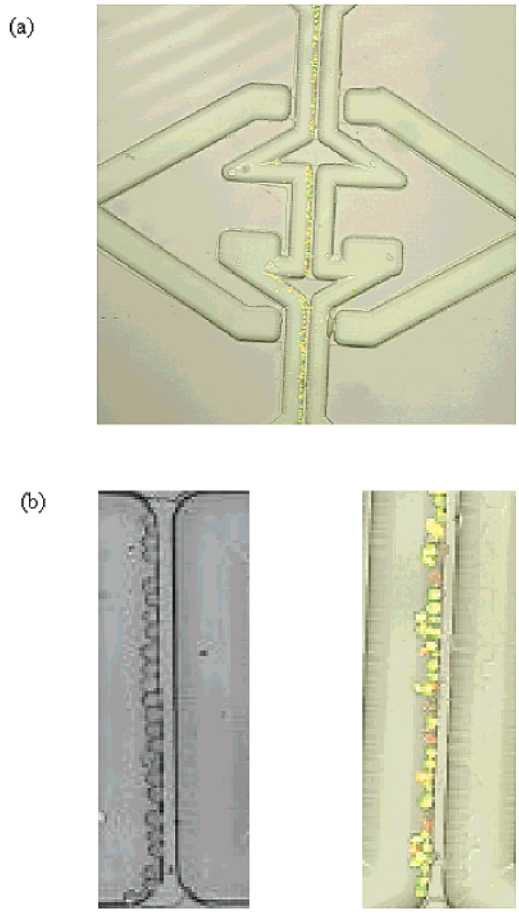

Figure 3. Cell docking and alignment on a microchip. (a) Fluorescence image of the microchannels showing the alignment of mammalian HL-60 cells along the dam structures. (b) Left: Photograph of a section of the dam with docked cells. A single layer of HL-60 cells was immobilized alone the dam with good integrity. Right: AO/EB staining of a line of HL-60 cells docked at the dam structure for 20 min. Most of the cells were stained by AO only (yellow), indicating that the cells were viable after docking.

were aligned on the dam in good integrity and round shape (Figure 3b, left), indicating the cells were not damaged during the docking process. To further confirm that the immobilized cells were alive after docking and prior to on-chip cell reactions, an AO/EB staining experiment was carried out 20 min after the docking procedure. Living cells were stained by AO and showed yellow fluorescence while dead cells were stained by both AO and EB and showed red fluorescence (Figure 3b, right). About 90% of the docked cells were stained only by the AO (a small percentage of cells are always dead under the culturing condition prior to docking), indicating that most of the cells were viable after docking.

The cell docking mechanism in this microfluidic device allows high-efficiency cell transportation and gentle immobilization of fragile mammalian cells. These features are significantly advantageous over the traditional perpendicular dams. The parallel dam structure is constructed along the main flow route and contributes minimal fluidic resistance against cell transportation. Meanwhile, fluidic pressure across the dam could be tuned by controlling the pressure difference between the two channels (channels 4 and 5 in Figure 2), an advantage for immobilizing fragile mammalian cells. As a result, cells can be transported in a considerably faster flow velocity in the direction of the main flow route than in the direction running toward the dam, making rapid cell transport and gentle cell docking possible. Once a cell is docked on a particular location of the dam, fluidic flow at that location experiences more resistance than that at other unoccupied locations. Cells driven by fluidic flow tend to dock on other regions until the dam is fully occupied. This dynamically changing liquid pressure initiated by cell docking leads to the formation of a single line of aligned HL-60 cells as shown in Figure 3. The automatic alignment of cells is another unique feature in particle immobilization by the parallel dam structure, providing a stable and reproducible environment for conducting biological experiments. First, the total number of cells docked by self-alignment can be reproducibly controlled by the length of the dam. Second, the formation of a single line of cells implies that the fluidic resistance along the main flow route is stable throughout the experiment, which enables flow quantity to be correctly estimated, a crucial factor for integrating concentration gradient in the microchannels.

Mathematical Model of Cell Immobilization. A mechanical model is established to compare the liquid pressure difference and shear stress on the immobilized cells between perpendicular and parallel dam systems. Parameters applying to both systems, such as hydrodynamic force (generated by liquid level difference), total resistance (excluding the dams and cell immobilization), and

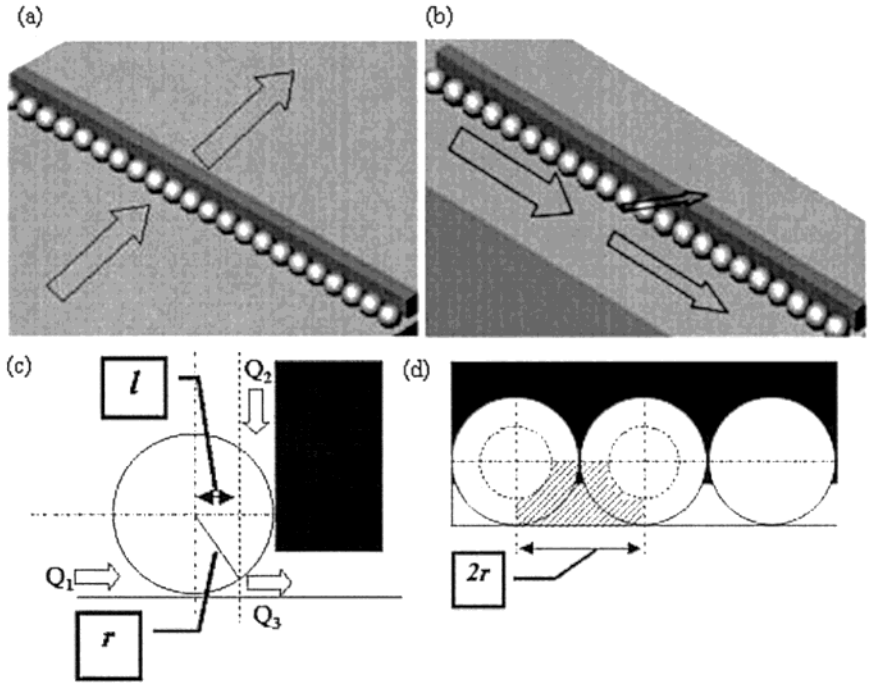

Figure 4. Mechanical model of fluidic stress on cells immobilized on different dam structures. (a) Schematic diagram showing the formation of multilayer cells due to accumulation of cells at a dam perpendicular to liquid flow. (b) Schematic diagram showing the formation of a single line of cells at a dam parallel to liquid flow. (c) Cross-sectional view showing the liquid flowing over the dam (Q_3) through two pathways (Q_1 and Q_2) and the fluidic resistance generated by the docked cell. (d) Calculation of the fluidic resistance of the docked cells by integrating the section areas blocking the liquid flow (the cellular part of the shadowed area). See text for detail.

dam lengths, are assumed to be identical based on the actual microdevice. The model also assumes that dam structures are constructed in the middle of both systems. Flow resistance caused by the unoccupied dams with only 10-μm width is negligibly small compared with the entire systems. Rigid, spherical-shaped beads of 15 μm in diameter (similar in size to HL-60 cells) are used to represent biological cells. Parts a and b of Figure 4 depict the formation of single-layer cells and the flow direction at a perpendicular dam and a parallel dam, respectively. In both cases, the immobilized cells are mainly subjected to two stresses: the liquid pressure difference across the immobilized cells that is related to flow resistance increment and the shear force caused by the liquid flow.

It is necessary to evaluate the increment in flow resistance caused by cell immobilization in both dam structures with respect to the total system resistance. The resistance is related to the total flow quantity, which is directly proportional to the liquid pressure difference across cells and the shear force. To calculate the resistance increment of a single layer of immobilized cells, the pathways for fluid flow through the layer should be clearly defined. Figure 4c depicts the front view of a simplified dam structure with a docked spherical particle. Liquid flowing across the dam will approach the particle via two pathways (opened arrows Q_1 and Q_2) and then combine to Q_3 before flowing across the dam. If the fluidic resistance in any of these pathways is R, the total resistance introduced by a spherical-shaped particle is 1.5R. According to hydrodynamic theory,[27]

$$R = C(L/S^2) \tag{1}$$

where C is a constant value related with fluid viscosity γ, L is the length, and S is the sectional area of the channel, respectively. The fluidic resistance in any of these three identical pathways is the integration of the intersection (shaded area in Figure 4d) from center of the sphere until $l = r$:

$$R = C\int_0^r \frac{\mathrm{d}l}{\{n[2r^2 - 0.5\pi(r^2 - l^2)]\}^2} \tag{2}$$

where r is the radius of the particle, n is the number of particles on the dam, and l is the point away from a sphere center at which the sectional area is integrated.

For a particle with a radius of 7.5 μm (such as an HL-60 cell), R is equal to $1.2 \times 10^{-5}C$. The increase in total fluidic resistance due to the immobilization of a single layer of particles on either the perpendicular dam or the parallel dam is $1.8 \times 10^{-5}C$. This is relatively small as compared to the total resistance in both flow systems ($\sim 2.0 \times 10^{-2}C$ based on the channel resistance from inlet 1 to outlet 5 of the actual microdevice with a cross section of 69 $\times$ 19.3 μm and a length of 2×10^4 μm, Figure 1b). Therefore, there is minimal impact on total flow quantity after the immobilization of a single layer of particles.

Change in the flow quantity across the immobilized particles (Q_m) depends on how the dams are constructed in each system. The relationship between Q_m and liquid pressure difference across the immobilized particles (ΔP_m) can be derived from the Bernoulli equation:[26]

(26) Yang, M.; Yang, J.; Li, C. W.; Zhao, J. *Lab Chip*, in press.
(27) Pnueli, D.; Gutfinger, C. *Fluid Mechanics*; Cambridge University Press: New York, 1992.

$$\Delta P_m = \rho g R_m Q_m \quad (3)$$

where ρ is the density of buffer, g the acceleration of gravity, R_m the dimensional parameters of the flow systems, and Q_m the flow quantity across the immobilized particles. The relationship between Q_m and shear force F is given by Stokes equation:[35]

$$F = 6\pi\mu r U_0 = 6\pi\mu r Q_m / A \quad (4)$$

where μ is the fluid viscosity, r the radius of the particle, U_0 the fluidic flow rate, and A the arbitrary cross-sectional area of the pathway generated by the immobilized particles (taken as the shaded area in Figure 4d multiplied by the number of immobilized cells on the dam). In Figure 4a, Q_m is equal to the total flow quantity because there is only one flow route in the perpendicular dam system. While for the parallel dam (Figure 4b), because the flow is split, the maximum flow quantity Q'_m passing through the particles docked on parallel dam is only half of the total flow quantity. According to eqs 3 and 4, ΔP_m and F (A value is identical in both dams for single-layer immobilization) are directly proportional to flow quantity Q_m. As a result, by splitting the flow route in the parallel dam system, the liquid pressure and the shear force experienced by the particles is at most half of that in the perpendicular dam system.

In practice, it is difficult to reproducibly generate a single layer of particles on perpendicular dams. Instead, beads usually form aggregate and multilayers at the dam as previously reported.[6] The fluidic resistance resulting from the formation of multilayer particles will significantly increase and eventually lead to clogging of the dam (where S approaches zero in eq 1). According to the above mechanical model, if two layers of particles are immobilized on the perpendicular dam, there will be at least a 40-fold increase in ΔP_m as compared to a single layer of particles. The increased pressure difference is probably the main reason for the distortion and leaking (squeezing through) of cells docked at the perpendicular dam.

Generation of Concentration Gradients. The network of microfluidic channels in the current device shown in Figure 1b was designed to generate a concentration gradient by controlled fluid distribution and diffusive mixing. Our preliminary work has demonstrated that an analyte solution could be diluted to different gradients as a function of distance along the dam.[26] In principle, analyte and buffer solutions were injected from different inlet vials into the microfluidic channels where they were mixed at different intersections (X and Y points in Figure 1b). The laminar property of flows in microchannels allows the analyte to diffuse into the fresh buffer in the downstream channel to form a continuous concentration gradient along the flow direction. By controlling flow rates and liquid pressures at different inlets, it is possible to generate a broad range of continuous and discontinuous gradients with variable resolutions along the microchannels.

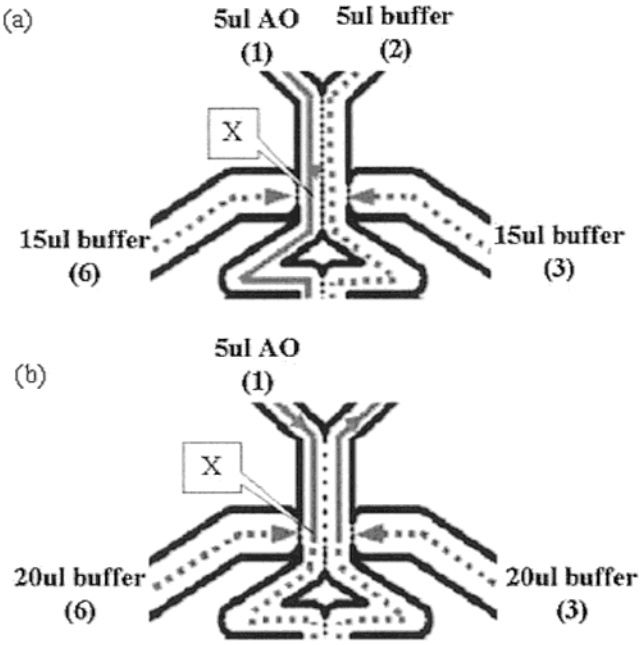

Figure 5. Schematic diagrams of flow directions and distribution within the microchannels when a dye solution is mixed with a buffer using (a) simple and (b) complex modes of controlled dilution program. The volumes of the dye solution and the buffer in each vial are indicated in the diagrams for each mode. The solid lines represent the flow route of the dye solution, and the dotted lines represent that of the buffer.

We have developed two liquid control modes to generate solutions of different concentration gradients. Figure 5 shows the flow directions and distribution within the microchannels when a dye solution is mixed with a buffer using two different modes of liquid level programs (Table 1, C1 and C2) to control the liquid pressure. In the simple dilution mode (Figure 5a), the analyte solution flowing from inlet 1 and the buffer from inlet 6 meet at intersection X. Because the liquid pressures between inlet 1 and inlet 2 and between inlet 3 and inlet 6 are equal (symmetrical), there is not net flow over the dam from channel 1 to channel 2 and vice versa (Table 1, C1). As a result, the two laminar flows at intersection X flow downstream along channel 1 side by side and diffusion is the main mixing mechanism during this period.[16] The mixed solution is further diluted in the intersection Y (Figure 1b) by the buffer such that the concentrations in the section before X (A−B), between X and Y (C−D), and after Y (E−F) are different. A discontinuous concentration gradient is generated in these sections ($[C]_{A-B} > [C]_{C-D} > [C]_{E-F}$). In addition, a continuous concentration gradient is generated in each section due to different degrees of diffusion along the channel.

In the complex dilution mode (C2 in Table 1), the analyte solution was introduced from inlet 1 and buffer was introduced from inlets 3 and 6, with inlet 2 remaining empty (Figure 5b). An asymmetrical pressure is generated between the inlets, where the higher liquid pressure in inlets 3 and 6 than in inlets 1 and 2 prevents the analyte solution from directly flowing into the

(28) Crank, J. *The Mathematics of Diffusion II*; Oxford University Press: Oxford, U.K., 1975.
(29) Hubley, M. J.; Locke, B. R.; Moerland, T. S. *Biochim. Biophys. Acta* **1996**, *1291*, 115−121.
(30) Montero, M.; Garcia-Sancho, J.; Alvarez, J. *Biochem. J.* **1995**, *305*, 879−887.
(31) Lee, H.; Suh, B.; Kim, K. *J. Biol. Chem.* **1997**, *272*, 21831−21838.
(32) Stutchfield, J.; Cockcroft, S. *FEBS Lett.* **1990**, *262*, 256−258.
(33) Marsigliante, S.; Giovanna Elia, M.; Di Jeso, B.; et al. *Cell. Signaling* **2002**, *14*, 61−67.
(34) Fairbaim, I. P.; Stober, C. B.; Kumararatne, D. S.; Lammas, D. A. *J. Immunol.* **2001**, *167*, 3300−3307.
(35) Gaver, D. P.; Kute, S. M. *Biophys. J.* **1998**, *75*, 721−733.

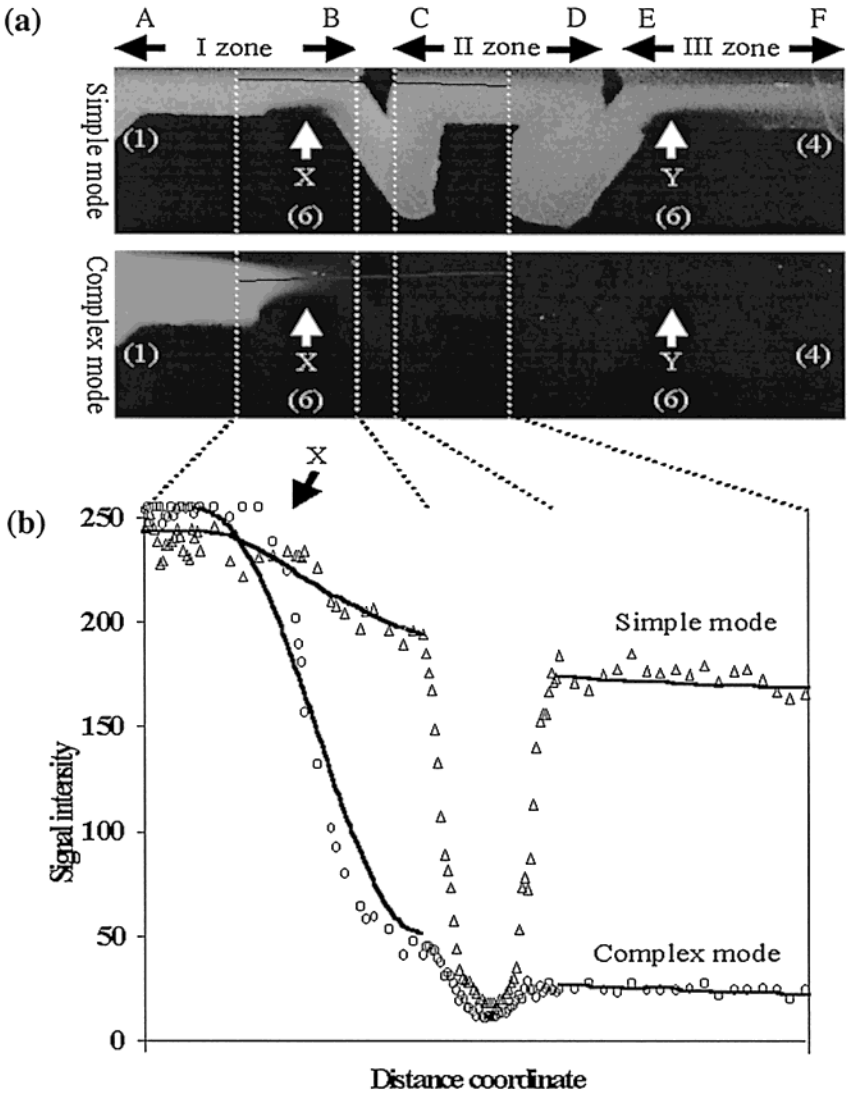

Figure 6. Generation of concentration gradients by flow distribution and diffusive mixing on the microchip. Two liquid pressure control modes were used in our experiments as shown in Figure 5. (a) Fluorescence images of the microchannels showing the dilution of an AO solution by PBS buffer using the (top) simple and (bottom) complex modes, respectively. The channels are labeled with numbers as in Figure 1b, and X and Y indicate the intersections where the AO solution and the buffer are mixed. (b) The concentration profiles of the AO solution along the channels generated by the simple (triangles) and complex (circles) modes of fluidic control. The fluorescence intensity was determined by scanning a line profile 10 μm from the dam. The solid lines represent the simulation results predicted based on the hydrodynamic diffusion model (eq 6).

downstream channel. The analyte solution and the buffer are mixed in intersection X and diffusion occurs at this converging point. As a result, only a small quantity of analyte will diffuse into the downstream channel to generate a steep, continuous concentration gradient in the sections after intersection point X (C−D and E−F).

Figure 6 shows the different concentration gradient profiles generated by the simple and complex dilution modes. The fluorescent dye AO was used for visualizing these gradient profiles. As described above, the difference between the simple and the complex modes is the dilution mechanism at the X intersection. For the simple mode (Figure 5a), the dilution process is similar to that in a T intersection.[14] AO solution from vial 1 and buffer from vial 6 were joined at intersection X and diffusively mixed along the channel downstream to generate a gradient. For the complex mode (Figure 5b), AO solution from vial 1 was forced to flow across the dam into vial 2 (which was empty). Only a small amount of AO solution would diffuse into the buffer stream, and a much greater dilution gradient was established in the downstream. The fluorescence images of the microchannels clearly show the different gradients of AO solution using the two dilution modes (Figure 6a). The fluorescence intensity determined by scanning a line profile 10 μm from the dam shows that, in the simple mode, the analyte was diluted to 80% of its original concentration between the A−B and C−D zones (Figure 6b, triangles). In the complex mode, however, a 15-fold dilution was observed between the same zones (Figure 6b, circles).

It is remarkable that a large dynamic range of concentration gradients could be generated by simply changing the liquid pressures in a single intersection, which provides a convenient method for serial dilution experiments. Previously reported microfluidic dilution architectures usually predetermined the dynamic range of dilution in a single intersection,[14,17] and altering liquid pressure only resulted in minimal change of the dynamic

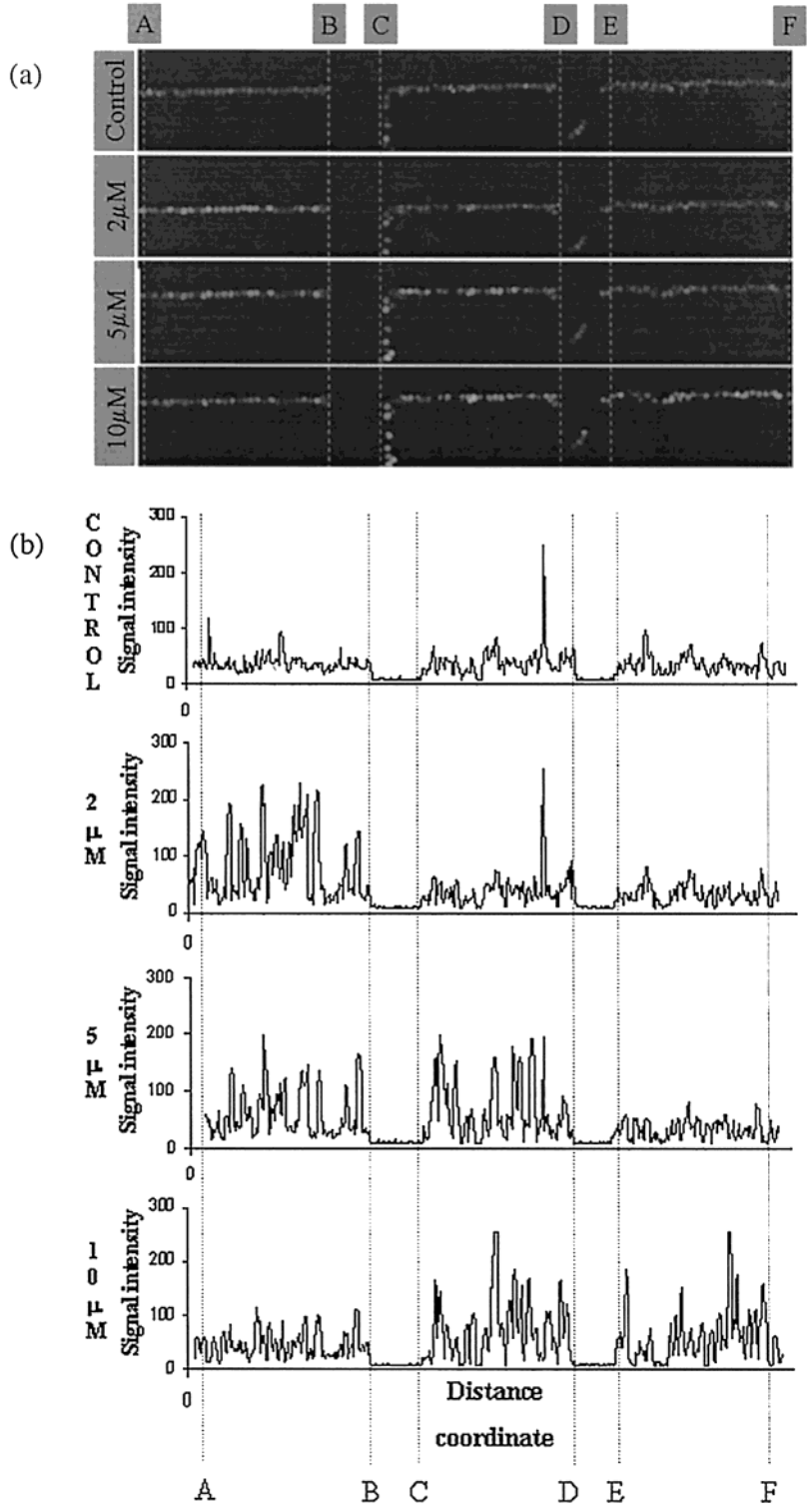

Figure 7. On-chip monitoring of ATP-dependent intracellular calcium uptake. (a) Fluorescence images of HL-60 cells prestained with calcium binding dye (Fluo3-AM) with the addition of different concentrations of ATP solutions. The ATP solution was diluted along the channels and dam structures by using the complex dilution mode. Points A−F are corresponding positions in Figure 6a. (b) Relative cellular fluorescence intensity of the docked cells shown in (a). The fluorescence intensity was determined by scanning a line profile across the line of cells docked at the dam. Signal intensity was increased by ~3-fold for ATP stimulated HL-60 cells, and the threshold concentration range for ATP-stimulated calcium uptake could be estimated based on the distance coordinate and eq 6.

range because of the fixed channel length ratio.[14] Another advantage of the current design is that consecutive dilution can be carried out within a small microscale feature (X and Y intersections in Figure 1c), which allows data acquisition by a single image scan to capture the whole gradient profile. In addition, regardless the dilution mode employed, two or more consecutive dilutions can be performed by subsequent intersections fabricated in the same microfluidic device.

A hydrodynamic model has been developed to describe the flow distribution in each intersection and diffusion process in downstream channels in the microfluidic network.[26] Similar to many microfluidic systems with low Reynolds number, the flow is laminar within the channels and a formula derived from Bernoulli equation can be applied to this microfluidic network,[26,27]

$$\Delta H = RQ + KQ^2 \tag{5}$$

where the liquid level difference ΔH and the flow quantity Q in each channel depend on the geometrical profile of the channels defined by fluid and dimensional parameters R and K. Taking into account the effect of diffusion, a mathematical equation can be established to calculate the concentration at any distance after lamina mixing,[28]

$$C(t, x) = \frac{1}{2}C_0 \sum_{n=-\infty}^{\infty} \left\{ \text{erf} \frac{h + 2nl - x}{2\sqrt{Dt}} + \text{erf} \frac{h - 2nl + x}{2\sqrt{Dt}} \right\} \tag{6}$$

where C(t, x) is the concentration at time t and at point x, D is the diffusion coefficient (for example, $D = 3.68 \times 10^{-6}$ cm^2/s for ATP[29]), l is the width of the channel, h is the width of the initial distribution, and C_0 is the concentration before intersection. Numerical simulation based on the model was used to compute the gradient profiles of the AO solution using the two dilution modes, and the calculated results agree well with the experimental observations (Figure 6b). A detailed description of the mathematical model of the microfluidic network and the approach to calculate the concentration profile of an analyte within the channels is reported in a separate paper.[26]

On-Chip Measurement of Threshold ATP Concentration. ATP-dependent calcium uptake was used as a model to demonstrate the capability of the microchip in monitoring a cellular response under a concentration range of a particular analyte of biological significance. This reaction model was chosen for two reasons. First, calcium ion mobilization induced by ATP is a dose-dependent reaction. The reaction is very sensitive at low ATP concentration, and a common sharp rise of calcium response is observed with increasing ATP concentration.[30,31] The minimum ATP concentration that induces significant calcium signal response is defined as the threshold concentration of this reaction. The availability of intracellular calcium-sensing molecules such as Fluo3-AM allows fluorescence intensity to be measured by a confocal fluorescence microscope. Second, the experiments were performed in a nonsterile area that required rapid reactions to prevent contaminations. ATP-induced calcium ion mobilization causes a biphasic response with rapid transient increase in signal intensity at the first phase.[31,32] ATP-dependent calcium uptake is a relatively fast reaction[33,34] but sufficient for our measurements (2 min after loading ATP on vial). In addition, the cellular reaction is reversible with the response returning to basal level quickly in the absence of extracellular calcium ions.

Cell docking and analyte concentration gradient were combined to determine the threshold concentration of ATP-dependent calcium uptake. The fluorescence images of the microchip under different conditions are shown in Figure 7a, with ~80 docked cells along the dam. Corresponding fluorescence intensity along the line of the docked cells is shown in Figure 7b. The HL-60 cells were preincubated with the calcium binding Fluo3-AM prior to docking at the parallel dam structure using the procedure described above. The background cellular signal detected in the "control" image was due to the presence of intracellular calcium in HL-60 cells. When an ATP solution (2 μM) was loaded into vial 1 and injected into the microchannels using the complex dilution mode (Table 1, D), the cellular signal intensity was increased by 3-fold in the A−B zone as compared to other zones (Figure 7, 2 μM image and line profile). It can be seen that the ATP threshold concentration was located between points B and C. After being washed with buffer, the same batch of docked HL60 cells was exposed to higher ATP concentrations. Using the same dilution mode, the threshold ATP concentration range shifted downstream with increasing analyte concentrations. With 5 μM ATP loaded into the microdevice, the cellular fluorescence intensity in both the A−B and C−D zones was enhanced (Figure 7, 5 μM image and line profile). In 10 μM ATP, the calcium-Fluo3 fluorescence in all docked cells was excited, where the relatively weak signal intensity at the A−B zone was due to the desensitization of calcium channels[30] by multiple ATP stimulations (Figure 7, 10 μM image and line profile).

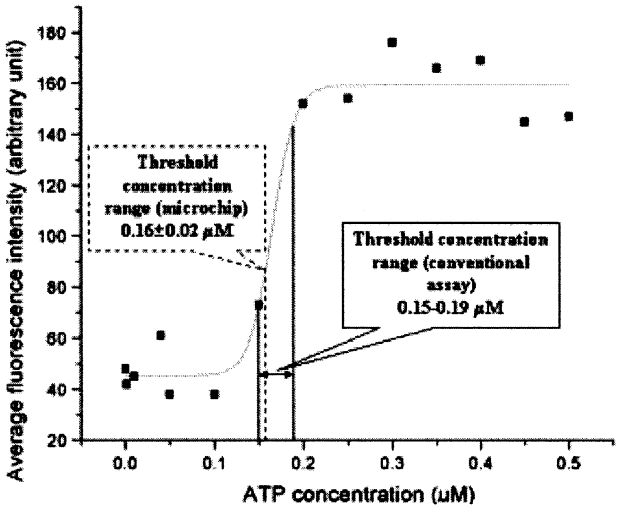

Figure 8. Determination of the threshold concentration range for ATP-stimulated calcium uptake by conventional serial dilution experiments. The estimated ATP threshold concentration from the microchip experiment is also shown.

The experimental results obtained above indicated that the threshold ATP concentration was at a range below 2 μM. Using the flow distribution and diffusion model described above (eqs 5 and 6), the ATP concentration gradient along the dam structure could be calculated. Based on the intensity results obtained in 2 and 5 μM ATP solutions, the threshold concentration was estimated to within a range of 0.16 ± 0.02 μM. The result is in good agreement with the threshold ATP concentration determined by using conventional fluorescence measurements. Figure 8 shows the fluorescence titration results obtained from 13 individual serial dilution experiments. The threshold concentration range was determined to be 0.15−0.19 μM.

In addition to the simplicity and reduction in reagent consumption and assay time, several advantages exist for on-chip measurement as compared to the conventional assay. With a small detection window covering a wide range of concentrations on the

microfluidic device, both fluorescence intensity maximums and minimums were easily captured by a single scan. Scanning parameters were identical throughout all concentrations. On the other hand, conventional assay requires repeat focus adjustment between every sample examination, which could contribute a considerable experimental error in fluorescence intensity reading where even a fine focus adjustment will significantly alter signal intensity. Furthermore, because of the small detection window, a much shorter scanning period is required for the on-chip measurement, which significantly enhances the data acquisition efficiency and reduces photobeaching effects of the fluorescence samples.

CONCLUSIONS

We have developed a microfluidic device that integrates cell docking and concentration gradient functions. To demonstrate the analytical capability and flexibility of the microchip, the threshold concentration of the ATP-dependent calcium uptake reaction was estimated in a single on-chip experiment, which is consistent with that obtained from the conventional assay involving 13 individual experiments. The microfluidic device described in this study allows rapid transportation and gentle immobilization of particles, particularly mammalian cells, in a controllable manner. Cells were immobilized by cell docking, which allowed suspension cells to align gently in a parallel dam without the need for complex microstructures or control devices. Docking process was dependent on cell concentration and was usually rapid and completed in several minutes. The microfluidics was also designed to generate a wide spectrum of concentrations. A large dynamic range of gradient could be established within a confined region, which facilitates all docked cells and the complete concentration range being inspected in a single confocal scan with high resolution. The integration of the cell manipulation and solution manipulation on a microchip provides an efficient and stable platform for the measurement of concentration-dependent biological responses within a confined microscale feature with improved reproducibility and reliability.

ACKNOWLEDGMENT

This work was partially supported by the Research Grants Council, Hong Kong and National Natural Science Foundation through a joint research scheme (N_CityU 114/99, Project 9050136). Helpful discussion with Prof. S. F. Sui of Tsinghua University is grateful acknowledged. We thank Dr. J. L. Zhao of Shanghai Institute of Microsystems and Information Technology, Chinese Academy of Science, for assistance in fabricating the quartz microchip substrate. We also acknowledge Dr. D. Leung for his advice in calcium-signaling experiments.

SUPPORTING INFORMATION AVAILABLE

Video clip showing the docking of HL-60 cells at a parallel dam structure. This material is available free of charge via the Internet at http://pubs.acs.org.

Received for review January 23, 2002. Accepted June 7, 2002.

AC025536C